Inorganic Chemistry

ARTICLE

pubs.acs.org/IC

Influence of Mixed Thiolate/Thioether versus Dithiolate Coordination on the Accessibility of the Uncommon +I and +III Oxidation States for the Nickel Ion: An Experimental and Computational Study

Marcello Gennari,[†] Maylis Orio,[‡,⊥] Jacques Pécaut,[§] Eberhard Bothe,[∥] Frank Neese,[‡,∥] Marie-Noëlle Collomb,*[,†] and Carole Duboc*[,†]

[†]Université Joseph Fourier Grenoble 1/CNRS, Département de Chimie Moléculaire, UMR-5250, Laboratoire de Chimie Inorganique Redox, Institut de Chimie Moléculaire de Grenoble FR-CNRS-2607, BP-53, 38041 Grenoble Cedex 9, France

[‡]Institute for Physical and Theoretical Chemistry Universität Bonn, Wegelerstrasse 12, D-53113 Bonn, Germany

[§]Laboratoire de Reconnaissance Ionique et Chimie de Coordination, Service de Chimie Inorganique et Biologique, (UMR E-3 CEA/UJF, FRE3200 CNRS), CEA-Grenoble, INAC, 17 rue des Martyrs 38054, Grenoble cedex 9, France

[∥]Max-Planck-Institut für Bioanorganische Chemie, Stiftstr. 34-36, D-45470 Mülheim an der Ruhr, Germany

Supporting Information

ABSTRACT: Sulfur-rich nickel metalloenzymes are capable of stabilizing Ni^{I} and Ni^{III} oxidation states in catalytically relevant species. In an effort to better understand the structural and electronic features that allow the stabilization of such species, we have investigated the electrochemical properties of two mononuclear N_2S_2 Ni^{II} complexes that differ in their sulfur environment. Complex **1** features aliphatic dithiolate coordination ([NiL], **1**), and complex **2I** is characterized by mixed thiolate/thioether coordination ([NiL^{Me}]I, **2I**). The latter results from the methylation of a single sulfur of **1**. The X-ray structure of **2I** reveals a distorted square planar geometry around the Ni^{II} ion, similar to what was previously reported by us for **1**. The electrochemical investigation of **1** and $\mathbf{2}^{+}$ shows that the addition of a methyl group shifts the potentials of both redox Ni^{II}/Ni^{I} and Ni^{III}/Ni^{II} redox couples by about 0.7 and 0.6 V to more positive values. Through bulk electrolyses, only the mononuclear dithiolate $[Ni^{I}L]^{-}$ ($\mathbf{1}^{-}$) and the mixed thiolate/thioether $[Ni^{III}L^{Me}]^{2+}$ ($\mathbf{2}^{2+}$) complexes were generated, and their electronic properties were investigated by UV−vis and EPR spectroscopy. For $\mathbf{1}^{-}$ (Ni^{I}, d^9 configuration) the EPR data are consistent with a $d_{x^2-y^2}$ based singly occupied molecular orbitals (SOMOs). However, DFT calculations suggest that there is also pronounced radical character. This is consistent with the small *g*-anisotropy observed in the EPR experiments. The spin population (Mulliken analysis) analysis of $\mathbf{1}^{-}$ reveals that the main contribution to the SOMO (64%) is due to the bipyridine unit. Time dependent density functional theory (TD-DFT) calculations attribute the most prominent features observed in the electronic absorption spectrum of $\mathbf{1}^{-}$ to metal to ligand charge transfer (MLCT) transitions. Concerning $\mathbf{2}^{2+}$, the EPR spectrum displays a rhombic signal with $g_x = 2.236$, $g_y = 2.180$, and $g_z = 2.039$ in CH_3CN. The g_{iso} value is larger than 2.0, which is consistent with metal based oxidation. The unpaired electron (Ni^{III}, d^7 configuration) occupies a Ni-d_{z^2} based molecular orbital, consistent with DFT calculations. Nitrogen hyperfine structure is observed as a triplet in the g_z component of the EPR spectrum with $A_N = 51$ MHz. This result indicates the coordination of a CH_3CN molecule in the axial position. DFT calculations confirm that the presence of a fifth ligand in the coordination sphere of the Ni ion is required for the metal-based oxidation process. Finally, we have shown that **1** exhibits catalytic reductive dehalogenation activity below potentials of −2.00 V versus Fc/Fc^{+} in CH_2Cl_2.

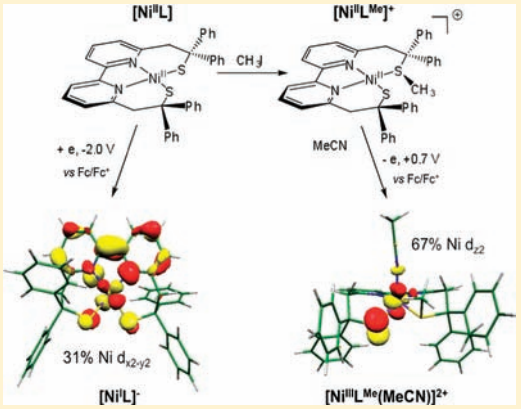

INTRODUCTION

Among the eight known nickel enzymes engaged in various redox activities,[1] four involve thiolate−nickel bonds in their active site. The Ni superoxide dismutase (NiSOD) catalyzes the disproportionation of superoxide radical anion into hydrogen peroxide and molecular dioxygen.[2−5] NiFe hydrogenase reversibly reduces protons to H_2.[6−8] CO dehydrogenase reversibly oxidizes CO to CO_2.[9−11] Finally, acetyl-CoA synthase produces acetyl-coenzyme A (acetyl-CoA) from CO, CoA, and a methyl group.[12−14] In these enzymes, the nickel sites exhibit extreme plasticity in both metal coordination and redox chemistry. In addition to the regular +II oxidation state of the thiolate−nickel

Received: January 11, 2011
Published: March 23, 2011

Scheme 1

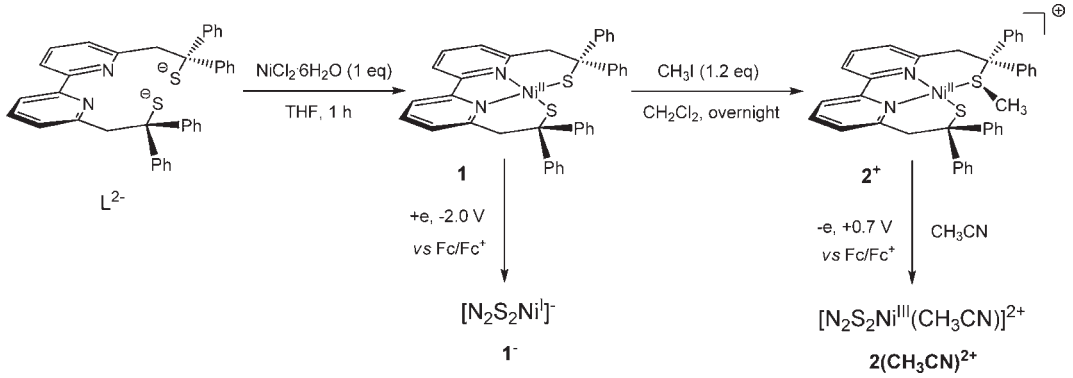

complexes, the uncommon +I and +III oxidation states are involved in several catalytically relevant species.

In view of elucidating the catalytic mechanisms of these sulfur-rich metalloenzymes, considerable efforts have been directed toward synthesizing low molecular weight Ni complexes that mimic some of the active site's structural, spectroscopic, and functional properties.[15−17] Importantly, a number of square planar dithiolate Ni^{II} compounds in an N_2S_2 coordination sphere have been described.[15] Their structural, electronic, and redox properties have been investigated in detail, as well as their reactivity in S-oxygenation[18−21] or/and S-alkylation[22−26] reactions. These studies have given insight into the nucleophilicity of the S-thiolate ligands versus the reaction products, i.e., S-oxygenated derivates or S-thioethers, respectively.

By contrast, substantially fewer studies were directed toward Ni^{III} thiolate complexes. To the best of our knowledge, a single example of such a species has been structurally characterized so far.[27] The other available reports concern *in situ* generated Ni^{III} complexes, either by chemical or electrochemical oxidation process of the corresponding Ni^{II} species.[15] The exploration of the electronic structure of these Ni^{III} complexes by EPR spectroscopy and DFT calculations has suggested a highly covalent character for the Ni−S bond, as well as a better stabilization of this oxidation state in a five- or six-coordinated environment compared to a square planar geometry.[19,28−33] However, the influence of a mixed thiolate/thioether environment on the electronic properties of the Ni^{III} ion has not been investigated in depth so far.[33,34]

Synthetic Ni^{I} thiolate complexes are even more sparse than those of Ni^{III} because of their instability with respect to disproportionation to Ni^{II} and Ni^{0} species.[35] Examples of structurally characterized mononuclear thiolate Ni^{I} complexes have only been reported in organometallic chemistry.[36] A few Ni^{I} thiolate complexes have been generated *in situ*. However this occurred exclusively from Ni^{II} complexes with aromatic thiolates[37−40] or with mixed sulfur environments (thiolate/thioether or thiolate/SO_2),[22] both of which are known for stabilizing the +I oxidation state. Furthermore, the investigation of the electronic properties of these Ni^{I} species has, until now, been very limited.[22,37,38,40] Consequently, to the best of our knowledge, no Ni^{I} complex in an aliphatic thiolate environment, as found in the mimicked metalloenzymes, has been reported.

It is thus of crucial importance to improve our knowledge on the electronic properties of Ni^{III} and Ni^{I} species with different types of aliphatic sulfur donors, e.g., pure thiolate versus mixed thiolate/thioether environments. We have recently reported the synthesis and characterization of a mononuclear diamine aliphatic dithiolate Ni^{II} complex, $[Ni^{II}L]$ (**1**) [L^{2-} = 2,2′-(2,2′-bipyridine-6,6′-diyl)bis(1,1-diphenylethanethiolate), Scheme 1], that does yield metal-based oxidation. Interestingly, upon electrochemical oxidation in the presence of imidazole (im), the square planar N_2S_2 Ni^{II} complex is converted into a square pyramidal N_3S_2 Ni^{III} complex, $[NiL(im)]^+$, thus mimicking the redox structural changes of NiSOD during its catalytic cycle.

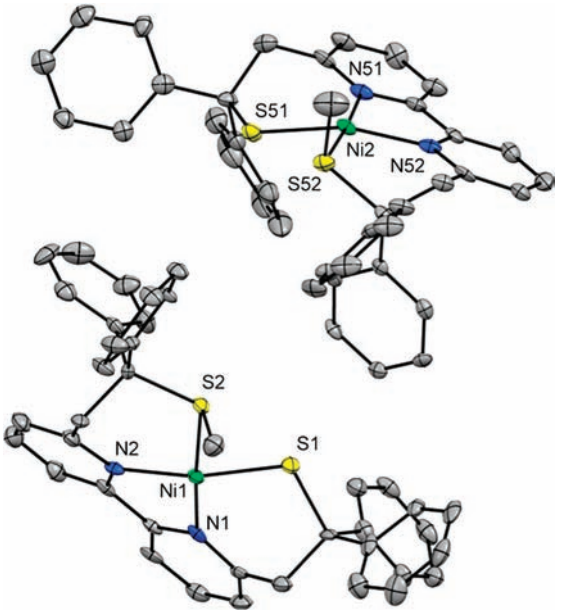

Figure 1. ORTEP drawing of the two independent molecules of $[NiL^{Me}]I\cdot 2H_2O$ (**2I**·$2H_2O$, 30% thermal ellipsoids). Hydrogen atoms, iodide counteranions, and water molecules are omitted for clarity.

We report here the isolation and structural characterization of the mixed thiolate/thioether $[Ni^{II}L^{Me}]I$ complex (**2I**), which results from the mono-S-methylation of **1** (Scheme 1). The redox chemistry of these two Ni^{II} complexes was investigated either in coordinating (CH_3CN or DMF)[41] or in noncoordinating (CH_2Cl_2) solvent, with particular attention given to the influence of the thiolate/thioether donors in the accessibility of the +I and +III oxidation states for the metal ion. Unexpectedly, the $[Ni^{III}L^{Me}]^{2+}$ (**2**$^{2+}$) complex with a mixed thiolate/thioether

dx.doi.org/10.1021/ic200063d |*Inorg. Chem.* 2011, 50, 3707–3716

Table 1. Selected Bond Lengths (Å) and Angles (deg) Issued from the X-ray Structures of $2I \cdot 2H_2O$ and 1 As Well As from Their Optimized Structures

$2I \cdot 2H_2O$			1		
	exptl	calcd		exptl[32]	calcd
Ni(1)−N(1)	1.899(8)	1.897	Ni−N(1)	1.934(2)	1.918
Ni(2)−N(51)	1.914(7)				
Ni(1)−N(2)	1.918(7)	1.934	Ni−N(2)	1.935(2)	1.918
Ni(2)−N(52)	1.959(8)				
Ni(1)−S(1)	2.169(3)	2.215	Ni−S(1)	2.173(1)	2.180
Ni(2)−S(51)	2.174(3)				
Ni(1)−S(2)	2.172(2)	2.223	Ni−S(2)	2.176(1)	2.180
Ni(2)−S(52)	2.187(2)				
N(1)−Ni(1)−N(2)	84.6(3)	83.4	N(1)−Ni-N(2)	84.56(7)	84.5
N(51)−Ni(2)−N(52)	85.0(3)				
N(1)−Ni(1)−S(1)	94.8(2)	94.2	N(1)−Ni-S(1)	98.73(5)	100.6
N(51)−Ni(2)−S(51)	98.0 (3)				
N(1)−Ni(1)−S(2)	173.7(2)	173.6	N(1)−Ni-S(2)	161.11(5)	157.5
N(51)−Ni(2)−S(52)	176.2(2)				
N(2)−Ni(1)−S(1)	162.3(2)	160.0	N(2)−Ni-S(1)	159.97(5)	157.6
N(52)−Ni(2)−S(51)	163.2(2)				
N(2)−Ni(1)−S(2)	98.2(2)	99.9	N(2)−Ni-S(2)	99.06(5)	100.6
N(52)−Ni(2)−S(52)	98.4(2)				
S(1)−Ni(1)−S(2)	80.78(9)	80.9	S(1)−Ni-S(2)	84.25(2)	83.1
S(51)−Ni(2)−S(52)	79.27(10)				

coordination sphere and the aliphatic dithiolate $[Ni^{I}L]^{-}$ ($\mathbf{1}^{-}$) complex were successfully obtained by exhaustive electrolysis. To the best of our knowledge, these two compounds represent the first examples of Ni^{I} and Ni^{III} species in such environments. Their electronic properties were investigated by UV−vis and EPR spectroscopies combined with DFT calculations. Finally, the capability of **1** to perform electrocatalytic reductive dehalogenation reactions in CH_2Cl_2 solutions is discussed.

RESULTS

1. Synthesis and Characterization of $[NiL^{Me}]^{+}$ (2^{+}). The mono S-alkylated $[NiL^{Me}]I$ complex (**2I**) was synthesized from the reaction of **1**[32] with 1.2 molar equiv of CH_3I in CH_2Cl_2 accompanied by a drastic change of the color solution, from violet to dark yellow (Scheme 1). This complex was obtained in a good yield as expected from previous studies demonstrating that the second S-alkylation occurs more slowly than the first one.[24,42,43] To avoid the presence of the electroactive iodide counteranion during the electrochemical investigation, this anion was exchanged by $CF_3SO_3^{-}$ (OTf^{-}) by adding 1 molar equiv of $AgCF_3SO_3$ in a **2I** solution, giving **2OTf** (see Experimental Section).

The ORTEP drawing of the two independent molecules present in the unit cell of **2I** is shown in Figure 1, and selected bond lengths and angles are given in Table 1 together with those of **1**. The Ni^{II} ion is in the center of a square plane in a $N_2S_{thioether}S_{thiolate}$ donor environment. Slight distortions are evidenced by the fact that the Ni, N, and S atoms are displaced from the mean NiN_2S_2 plane from 0.07 to 0.20 Å. The six-membered nickel-aza-thiacyclohexane ring in **2I** obviously leads to larger deviation from planarity with respect to the more common five-membered nickel-aza-thiacyclopentane ring complexes.[21,23]

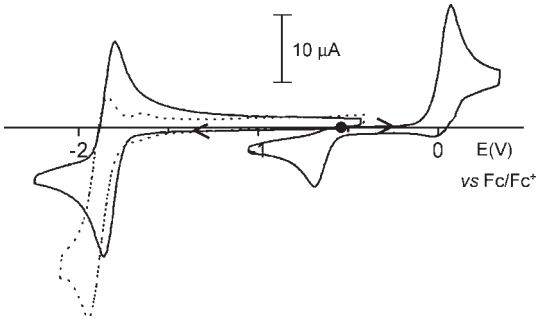

Figure 2. CV of **1** (1.6 mM) in DMF (—) and in CH_2Cl_2 (···), 0.1 M Bu_4NPF_6 at room temperature. Scan rate of 100 $mV \cdot s^{-1}$.

The nearest iodide is located at a distance of 3.778 Å from the nickel (Ni1), showing that the anion is not coordinated to the metal.

The Ni−S bond lengths are not very sensitive to the nature of the S-donor ligand, with the $Ni-S_{thiolate}$ bond being slightly shorter than the $Ni-S_{thioether}$ one. In contrast, the Ni−N bond *trans* to the thioether is shorter than the bond *trans* to the thiolate, as previously observed in other monomethylated N_2S_2 Ni^{II} complexes.[21,23,24] Upon S-methylation of **1** into 2^{+}, a stronger sensitivity of the Ni−S distances than the Ni−N ones would be expected because of the weaker σ-donor character of the neutral thioethers than the anionic thiolates. However, the invariance of the Ni−S bond length upon S-alkylation is attributed to a relief of the $d_{\pi}-p_{\pi}$ antibonding interaction between the metal and sulfur.[22,24,25,44,45]

The S-methylation of **1** leads to the closure of the S−Ni−S angle (about 4°), while no significant changes are observed in the

dx.doi.org/10.1021/ic200063d |*Inorg. Chem.* 2011, 50, 3707–3716

Table 2. Electrochemical Potentials for 1 and 2^+ at Room Temperature (vs Fc/Fc^+, 100 $mV \cdot s^{-1}$)

complex	solvent	oxidation process $Ni^{II} \rightarrow Ni^{III}$	reduction process $Ni^{II} \rightarrow Ni^{I}$
[NiL] (**1**)	DMF	Ep_a = +0.05 V; Ep_c = −0.73 V	$E_{1/2}$ = −1.85 V (ΔEp = 70 mV)
[NiL] (**1**)	CH_2Cl_2	Ep_a = +0.13 V; Ep_c = −0.55 V	$E_{1/2}$ = −1.90 V (ΔEp = 130 mV)
$[NiL^{Me}]^+$ ($\mathbf{2}^+$)	CH_3CN	$E_{1/2}$ = +0.60 V (ΔEp = 70 mV)	$E_{1/2}$ = −1.19 V (ΔEp = 60 mV)
$[NiL^{Me}]^+$ ($\mathbf{2}^+$)	CH_2Cl_2	$E_{1/2}$ = +0.68 V (ΔEp = 140 mV)	$E_{1/2}$ = −1.22 V (ΔEp = 100 mV)

Scheme 2

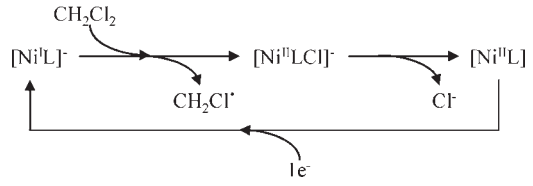

N−Ni−N angle (less than 0.5°). The $S-C_{CH3}$ distance of 1.858(9) Å is also typical.[25]

2. Electrochemical Properties of Complexes [NiL] (1). We have previously reported the redox properties of complex **1** in CH_2Cl_2.[32] The cyclic voltammogram (CV) displays two one-electron metal based processes: a poorly reversible Ni^{II}/Ni^{I} reduction wave at $E_{1/2}$ = −1.91 V versus Fc/Fc^+ and an irreversible Ni^{III}/Ni^{II} oxidation peak at Ep_a = +0.13 V.[46] The Ni^{III} complex undergoes a fast chemical reaction leading to a Ni^{III} dimer, which is irreversibly reduced at Ep_c = −0.55 V. In the presence of imidazole, the electrochemically oxidized species was characterized as a mononuclear $[Ni^{III}L(im)]^+$ complex.

In this work, the reduction properties of **1** were further investigated in DMF and CH_2Cl_2. The CV of **1** in DMF is analogous to that observed in CH_2Cl_2 (Figure 2). We can however notice slight potential shifts of the redox systems, and a better reversibility of the Ni^{II}/Ni^{I} reduction process in DMF (Table 2). The poor reversibility of this wave in CH_2Cl_2 arises from catalytic reductive dehalogenation of the solvent. This has been evidenced when a potential of −2.00 V versus Fc/Fc^+ is applied on a CH_2Cl_2 solution of **1**. First, a lack of current decrease is observed upon this applied potential. Second, when total charge (Q) approached a calculated value of 8 electrons per initial **1** complex, the CV of the solution is similar to the initial one except for the appearance of an irreversible oxidation peak at 0.8 V corresponding to the electroactivity of the released chloride anions. Furthermore, the amount of involved electrons exactly corresponds to the produced amount of Cl^-. On the basis of these data together with those of the literature, the mechanism displayed in Scheme 2 may be proposed.

The one-electron reduced form of **1**, $[NiL]^-$ ($\mathbf{1}^-$), can be afforded by a bulk electrolysis carried out at room temperature (E = −1.96 V) in DMF (Figure S2). Upon the reduction process, the solution changes from violet to brown with the appearance of two intense transitions at 25 000 and 21 050 cm^{-1}, as well as two less intense transitions at 12 350 and 11 100 cm^{-1} (Figure 3). The intensity of these electronic transitions is maximal after the exchange of 1.75 electrons per molecule of **1**. This excess of coulometry is proposed to be the result of the spontaneous reoxidation of $\mathbf{1}^-$ to **1** in the course of the electrolysis. This occurs without any degradation of the complex as attested by the CV recorded at the end of the electrolysis (Figure S2). From chronoamperometry, $\mathbf{1}^-$ is generated with an estimated yield of

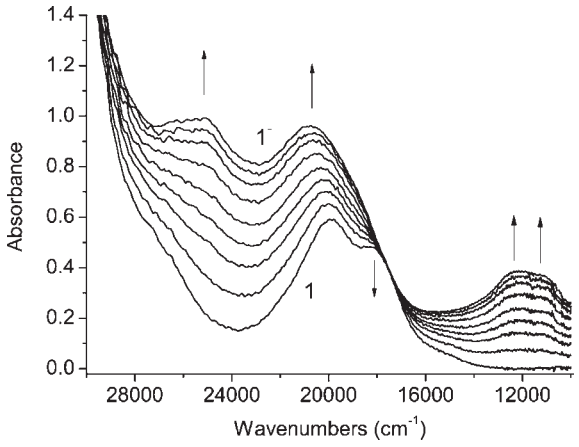

Figure 3. Evolution of the absorption spectrum of **1** (0.16 mM, 1 cm optical path) in DMF, 0.1 M Bu_4NPF_6 during the exhaustive electrolysis at −1.96 V vs Fc/Fc^+ at room temperature (time between two spectra: Δt = 2 min).

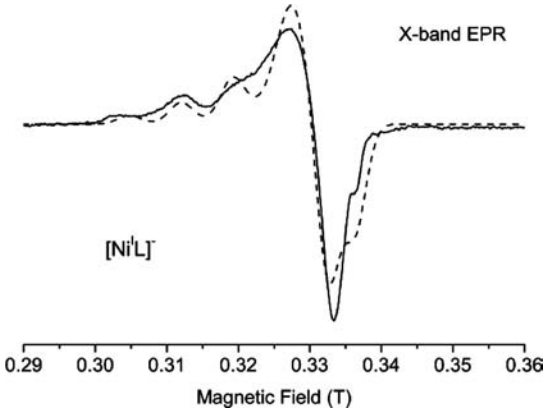

Figure 4. Experimental (—) and simulated (---) X-band EPR spectra (30 K) of $\mathbf{1}^-$, electrogenerated from a solution of **1** (0.15 mM) at −25 °C in CH_2Cl_2, 0.1 M Bu_4NPF_6. Parameters used for the simulation: $g_{\|}$ = 2.110, $g_{\perp}$ = 2.034, $A_{\|}$ = 212 MHz, $A_{\perp}$ = 32 MHz.

90%. In CH_2Cl_2, the same Ni^{I} species can also be produced in a comparable amount, but only at low temperature (Figure S3).

Finally, the metal based character of the process is confirmed by EPR spectroscopy. The frozen solution EPR spectrum of an electrogenerated solution of $\mathbf{1}^-$ in DMF or CH_2Cl_2 (Figure 4) displays an axial signal with $g_{\|} > g_{\perp} > 2.0023$, typical of Ni^{I} complexes having an $S = {}^1/_2$ ground state with the unpaired electron (d^9 for a Ni^{I} ion) occupying a predominantly $d_{x^2-y^2}$ orbital.[26,47,48] However, owing to the small anisotropy of g ($g_{\perp}$ = 2.034, $g_{\|}$ = 2.110), some radical character of the species is suggested. Five ^{14}N hyperfine lines are observed on the $g_{\|}$ component, consistent with the delocalization of the spin density

dx.doi.org/10.1021/ic200063d |Inorg. Chem. 2011, 50, 3707–3716

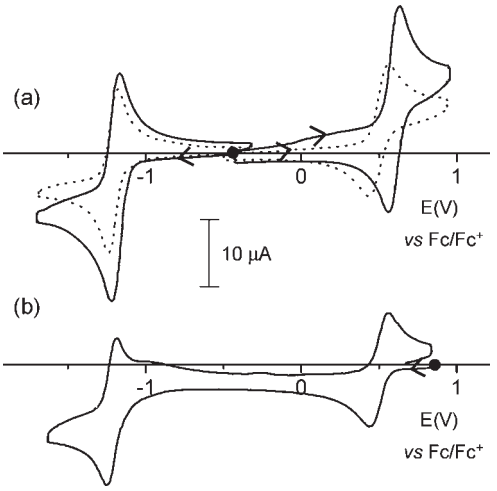

Figure 5. CV of **2OTf** (1 mM) in CH_3CN, 0.1 M Bu_4NPF_6 (a) at room temperature (—) and at ∼ −30 °C (···) and (b) after exhaustive electrolysis at +0.70 V at ∼−30 °C. Scan rate of 100 mV s^{-1}.

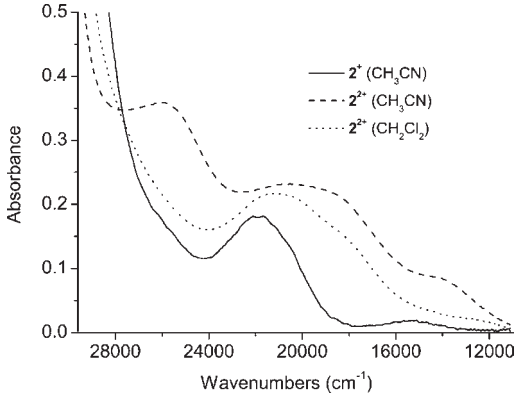

Figure 6. Absorption spectra of $\mathbf{2}^+$ (1 mM) in CH_3CN and of $\mathbf{2}^{2+}$, electrogenerated from 1 mM solutions of $\mathbf{2}^+$ (CH_3CN or CH_2Cl_2, 0.1 M Bu_4NPF_6) (1 mm optical path).

of the unpaired electron over the bipyridine units (two nitrogen atoms).

3. Electrochemical Properties of Complexes $[NiL^{Me}]^+$ ($\mathbf{2}^+$). The redox properties of $\mathbf{2}^+$ have been investigated in CH_3CN and CH_2Cl_2. The CV of $\mathbf{2}^+$ in CH_3CN (Figure 5a) displays two reversible one-electron metal based processes: a Ni^{II}/Ni^{I} reduction wave at $E_{1/2}$ = −1.19 V, and a Ni^{III}/Ni^{II} oxidation wave at $E_{1/2}$ = +0.60 V. By cycling at lower potential values, a second poorly reversible reduction wave at Ep_c = −2.00 V is observed that might be attributed to a metal or ligand based reduction process (Figure S4). As for **1**, the nature of the solvent (CH_3CN versus CH_2Cl_2) slightly affects the potentials of the redox systems of $\mathbf{2}^+$ (Table 2), and the Ni^{II}/Ni^{I} reduction wave is also less reversible in CH_2Cl_2 (Figure S5).

A comparison with the potential values of **1** shows that the addition of a methyl group induces a positive potential shift for both redox Ni^{II}/Ni^{I} and Ni^{III}/Ni^{II} systems of about 0.7 and 0.6 V, respectively. This potential shift is consistent with the decreased donor ability of the sulfur upon S-alkylation and with the development of positive charge on the mono-S-methylated complex.[22,24,25]

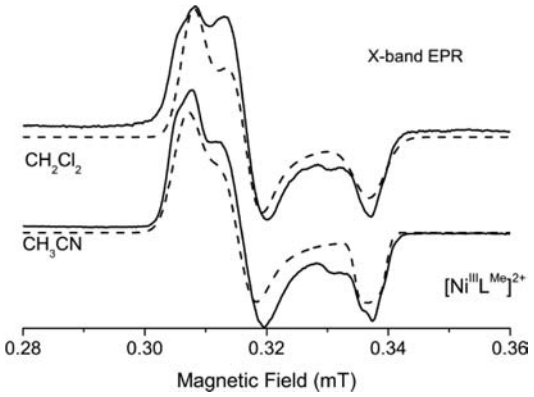

Figure 7. Experimental (—) and simulated (---) X-band EPR spectra (100 K) of $\mathbf{2}^{2+}$, electrogenerated from 1 mM solutions of $\mathbf{2}^+$ (CH_3CN or CH_2Cl_2, 0.1 M Bu_4NPF_6).

Upon examination of first the reduction of $\mathbf{2}^+$, although the Ni^{II}/Ni^{I} wave appears reversible in CH_3CN, and the corresponding redox potential that is less negative by 0.7 V compared to that of **1**, an exhaustive reduction of the solution at room temperature (E = −1.35 V) shows that the reduced Ni^{I} species (**2**) is not stable. Indeed, at the end of the electrolysis (about 1 electron consumed), the resulting CV shows the disappearance of the initial Ni^{II}/Ni^{I} and Ni^{III}/Ni^{II} waves while several waves corresponding to undefined electroactive species appeared. Attempts to stabilize the reduced Ni^{I} species by performing reductive electrolysis at low temperature have failed.

Regarding the oxidation process, when an electrolysis at +0.70 V of a CH_3CN solution of $\mathbf{2}^+$ is carried out at room temperature, one electron per initial complex is exchanged. The CV of the resulting solution shows the nearly complete disappearance of the Ni^{III}/Ni^{II} wave at $E_{1/2}$ = +0.60 V, and the appearance of a shoulder at Ep_c = −1.00 V that precedes the Ni^{II}/Ni^{I} reduction wave of $\mathbf{2}^+$ (Figure S6). This demonstrates the instability of $[Ni^{III}L^{Me}]^{2+}$ ($\mathbf{2}^{2+}$) at room temperature and its chemical conversion to another electroactive species. It is proposed that $\mathbf{2}^{2+}$ decomposes *via* the formation of an intermediate thiyl radical leading to an S−S bond. This chemical transformation is reversible since an exhaustive reduction of the oxidized solution carried out at −1.10 V restores $\mathbf{2}^+$ *via* disulfide reduction, with a yield of about 80% (Figure S6).

However, if exhaustive oxidations of $\mathbf{2}^+$ are carried out at low temperature (∼−30 °C), the mononuclear $\mathbf{2}^{2+}$ complex is almost quantitatively generated either in CH_3CN (E = +0.70 V) or in CH_2Cl_2 (E = +0.89 V) (exchange of one electron per $\mathbf{2}^+$) (Figures 5b and S5b). Upon oxidation, the color of the solution turns from dark yellow to red. The resulting absorbance and EPR spectra are slightly different in both solvents, possibly due to the coordination of either a CH_3CN molecule or a triflate counteranion (in CH_2Cl_2) to $\mathbf{2}^{2+}$. In CH_2Cl_2, the spectrum exhibits two main transitions at 21 350 and 18 870 cm^{-1} (shoulder), while in CH_3CN additional transitions are observed at 26 320 and 13 700 cm^{-1} (Figure 6). The EPR spectra of $\mathbf{2}^{2+}$ recorded in both solvents are consistent with a mononuclear Ni^{III} species (Figure 7). The frozen solution spectra were simulated with the following parameters: g_x =2.238, g_y = 2.178, g_z = 2.039 in CH_3CN and g_x =2.231, g_y = 2.172, g_z = 2.039 in CH_2Cl_2. The g_{iso} values significantly larger than 2.0 are consistent with an $S = {}^1/_2$ ground state for the Ni^{III} species with the unpaired electron (d^7 for a Ni^{III} ion)

dx.doi.org/10.1021/ic200063d |*Inorg. Chem.* 2011, 50, 3707–3716

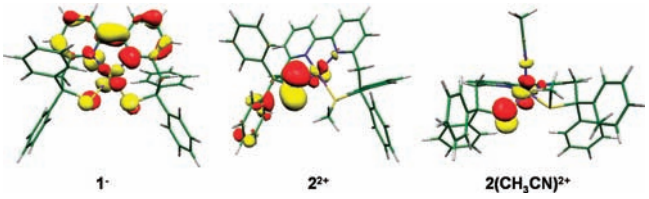

Figure 8. Localized SOMOs for $\mathbf{1}^{-}$, $\mathbf{2}^{2+}$, and $\mathbf{2(CH_3CN)}^{2+}$ complexes.

occupying a predominantly Ni-d_{z^2} orbital.[49] It has been shown that the Ni^{III} state is stabilized by interactions with donor axial ligand(s). This is confirmed by the EPR spectrum recorded in CH_3CN. The overall EPR spectral envelope is similar to that in CH_2Cl_2, with the exception of the three ^{14}N hyperfine lines imposed in the g_z component with A_N = 51 MHz. The triplet is compatible with the coordination of one CH_3CN molecule in the axial coordination site of a *z*-axis elongated square pyramid.[27,29,33] In CH_2Cl_2, the assumption that the fifth ligand (such as a water molecule or a triflate anion) is sufficiently coordinating to interact with the Ni^{III} ion would account for the identical position of the g_z signal in both solvents.

4. Electronic Structure of $[Ni^{I}L]^{-}$ ($\mathbf{1}^{-}$) and $[Ni^{III}L^{Me}]^{2+}$ ($\mathbf{2}^{2+}$) and Interpretation of Their Spectroscopic Properties. To obtain some insight into the geometrical and electronic structure of the Ni^{I} complex, $\mathbf{1}^{-}$, DFT calculations were carried out. Comparison between the optimized structures of **1** and $\mathbf{1}^{-}$ reveals a comparable environment around the nickel ion. Nevertheless, the reduction of the Ni ion engenders an overall expected expansion of its coordination sphere with longer Ni−N/S distances of about 0.01 and 0.04 Å, respectively (Table S2). Upon examination of the electronic structure of this Ni^{I} species, the singly occupied molecular orbital (SOMO) of $\mathbf{1}^{-}$ indicates a strong delocalization of the unpaired electron over the metal and the ligand, and especially over the bipyridine unit (Figure 8). The Mulliken population analysis further supports that the spin density is spread all over the complex since positive spin populations are found at the Ni ion (0.31), and the bipyridine unit (0.69 with 0.14 on each nitrogen atom) (Table S3). The dominant contribution of the bipyridine unit to the total spin density provides evidence for partial radical character for the $\mathbf{1}^{-}$ species, which is consistent with the experimental EPR data. Interestingly, a non-negligible part of the unpaired electron is located in the Ni $d_{x^2-y^2}$ metal-based MO. On the other hand, the low sulfur contribution to the SOMO indicates a limited degree of covalency for the Ni−S bond in contrast to what is observed in the previously described thiolate Ni^{II} and Ni^{III} complexes.[30,31,33]

The EPR parameters calculated on the optimized structure of $\mathbf{1}^{-}$ (g_x = 2.000, g_y = 2.025, and g_z = 2.107) are in very good agreement with experiment and confirm the validity of the DFT results for this Ni^{I} species (Table S4).

For a better understanding of the optical properties of $\mathbf{1}^{-}$, TD-DFT calculations were undertaken on its optimized structure. By employing this computational method, we can provide the assignment of its salient features by calculating the main transition energies and their relative intensities. Our calculations adequately reproduce the key features of the spectrum in terms of energy and intensity, namely, the two intense bands at 25 000 and 21 050 cm^{-1} (calc: $\lambda_{max}(f)$ = 24 752 (0.019) and 20 964 (0.044) cm^{-1}, respectively) and the shoulder at 18 800 cm^{-1} (calc: $\lambda_{max}(f)$ = 18 657 (0.011) cm^{-1}) (Table S5). Regarding the nature of these absorptions, Figure 9 shows that they all arise

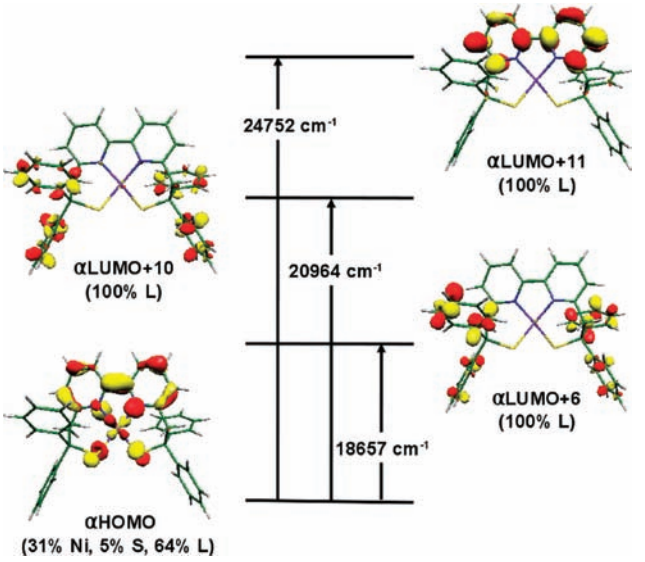

Figure 9. TDDFT assignment of the calculated transitions for $\mathbf{1}^{-}$ in CH_2Cl_2. The population of the relevant MOs (HOMO: highest occupied molecular orbital; LUMO, lowest unoccupied molecular) is indicated in parentheses as well as the wavelength of the optical transitions. Legend: Ni represents the metal, S the sulfur atoms, and L the rest of the ligand.

mainly from metal-to-ligand charge transfer (MLCT) transitions since the donor orbital is mainly metal-centered. For the transitions at 18 657 and 20 964 cm^{-1}, the acceptor orbitals are ligand-based MOs that are fully delocalized over the four phenyl groups of L. In the case of the 24 752 cm^{-1} transition, the acceptor orbital is also ligand-based but features a dominant contribution from the carbon atoms of the bipyridine unit.

DFT calculations were also undertaken to model the electronic and geometrical structure of the Ni^{III} complex, $\mathbf{2}^{2+}$. When looking at the electronic structure of the optimized Ni^{III} species initiated from the X-ray structure of $\mathbf{2}^{+}$, we observe that DFT calculations predict the single unpaired electron to mainly reside in a S(π)-based MO (Figure 8). In fact, the SOMO of $\mathbf{2}^{2+}$ features a large contribution from the thiolate unit (46%), which dominates over the Ni character (19%). This is further confirmed by the Mulliken population analysis showing that the thiolate bears most of the spin density with positive spin populations found at the S(1) atom (0.54), and the Ni ion (0.18) (Table S6). Consequently, this electronic structure may best be described as consisting of a Ni^{II}−thiyl radical species. This result is in complete disagreement with the EPR spectroscopic data recorded on the one-electron oxidized solution of $\mathbf{2}^{+}$ (Table S4 and Figure 7). Moreover, it is worth noting that a similar result was previously obtained from DFT calculations performed on a diamine dithiolate Ni^{III} complex which showed that the addition of a fifth ligand was necessary to reproduce the spectroscopic properties of this complex.[31]

To be consistent with the spectroscopic data, CH_3CN solvent molecules in our subsequent computational models of $\mathbf{2}^{2+}$ were thus explicitly included. The best geometry optimized model, namely $\mathbf{2(CH_3CN)}^{2+}$, is generated with only one CH_3CN ligand coordinated to an axial position of the Ni ion featuring a $Ni-N_{CH3CN}$ distance of 2.108 Å (Table S6). The computed electronic structure of this latter species correctly places the

dx.doi.org/10.1021/ic200063d |*Inorg. Chem.* 2011, 50, 3707–3716

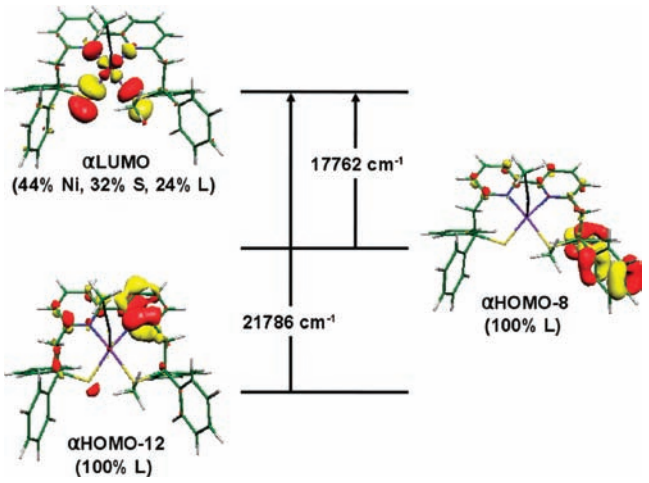

Figure 10. TDDFT assignment of the calculated transitions for $\mathbf{2}(CH_3CN)^{2+}$ in CH_2Cl_2. The population of the relevant MOs (HOMO, highest occupied molecular orbital; LUMO, lowest unoccupied molecular orbital) is indicated in parentheses as well as the wavelength of the optical transitions. Legend: Ni represents the metal, S the sulfur atoms, and L the rest of the ligand.

unpaired electron in the Ni(d_{z^2})-based MO (Figure 8). The SOMO of $\mathbf{2(CH_3CN)^{2+}}$ is thus primarily metal-based (67%) with a non-negligible contribution from the thiolate (20%), consistent with the EPR data (Table S3). As previously observed, the conversion of a square planar geometry to a square pyramidal environment drastically stabilizes the Ni^{III} state.[32]

The computed EPR parameters for $\mathbf{2(CH_3CN)^{2+}}$ (g_x =2.237, g_y = 2.162, g_z = 2.070, and A_N = 44 MHz) are in good agreement with the experimental data, thus validating $\mathbf{2(CH_3CN)^{2+}}$ as the one-electron oxidized species of $\mathbf{2}^+$. We note in passing that the EPR parameters calculated for $\mathbf{2}^{2+}$ without any axial ligand display very small g anisotropy, consistent with a radical based system (Table S4). This provides further evidence that this species does not represent the situation present in solution. .

TD-DFT calculations were undertaken on $\mathbf{2(CH_3CN)^{2+}}$ in order to assign the two main absorptions of its electronic spectra, i.e., the two bands at 21 350 and 18 870 cm^{-1}. The calculations nicely reproduce these key features in the spectrum in terms of energy and intensity (calc: $\lambda_{max}(f)$ = 21 786 (0.017) and 17 762 (0.012) cm^{-1}, respectively) (Table S7). Regarding the nature of these absorptions, Figure 10 shows that they all arise mainly from ligand-to-metal charge transfer (LMCT) transitions since the acceptor orbital is mainly metal-centered (44% Ni contribution). The donor orbitals of both absorptions are delocalized π-orbitals but feature completely different compositions. While the main contribution to the donor orbital of the 21 786 cm^{-1} transition comes from one pyridine ring of the bipyridine unit, the donor orbital of the 17 762 cm^{-1} transition is delocalized over the two phenyl rings of the thioether arm.

FINAL REMARKS AND CONCLUSIONS

Given the relevance of the uncommon thiolate Ni^I and Ni^{III} species in the catalytic cycle of sulfur rich Ni enzymes, we have sought to improve our understanding on the stability of such complexes through the examination of their electronic structure with different chemical environments, namely pure aliphatic thiolate versus mixed thiolate/thioether.

It has been previously observed that the Ni^I oxidation state is stabilized upon conversion of thiolate(s) to thioether(s), while the Ni^{III} oxidation state is destabilized in the cationic thioether derivatives.[22−26] This behavior has been explained by the loss of a $S_{p\pi}$−$Ni_{d\pi}$ antibonding interaction in the Ni−SR HOMO, and by the increase of the positive charge on the complex.[23,24,44,45] Unexpectedly, in this work, we were able, with the help of the ligands L and L^{Me}, to stabilize a mononuclear dithiolate $[Ni^IL]^-$ ($\mathbf{1}^-$) complex and a mixed thiolate/thioether $[Ni^{III}L^{Me}]^{2+}$ ($\mathbf{2}^{2+}$) complex. All of our attempts to generate either the dithiolate $[Ni^{III}L]^+$ ($\mathbf{1}^+$) complex in the absence of a strong donor ligand such as imidazole or the mixed thiolate/thioether $[Ni^IL^{Me}]$ ($\mathbf{2}$) species have failed.

The surprising stability of $\mathbf{1}^-$, which represents the first example of a Ni^I with a purely aliphatic dithiolate N_2S_2 environment, can be explained by the presence of the bipyridine ligand, which allows for the partial delocalization of the electron density onto coordinated ligand. In fact, the significant radical character of $\mathbf{1}^-$ was attested to by the small g-anisotropy, and the composition of the redox active molecular orbital of the complex (64% of the SOMO is localized on the bipyridine unit). The stability of $\mathbf{1}^-$ can also be related to the higher reduction potential of $\mathbf{1}$ (about −1.25 V vs NHE for the Ni^{II}/Ni^I redox system) with respect to the other previously reported N_2S_2 dithiolate Ni^{II} complexes (around −2.0 V vs NHE).[24] Furthermore, the Ni^{II}/Ni^I potential value of $\mathbf{1}$ falls near those of the mixed thiolate/thioether Ni^{II} complexes (between −1.18 and −1.37 V vs NHE), for which the corresponding Ni^I species were generated.[50,51]

Regarding $\mathbf{2}^{2+}$, this is the first example of a mononuclear Ni^{III} complex in a mixed thiolate/thioether environment. An earlier study of Brunold et al.[30] reports the investigation of the electronic structures of Ni^{III} complexes with pure thiolate S_4N_2 or S_2N_2 environments by several spectroscopic techniques and DFT calculations. They have also observed that addition of solvent is required to get optimized structures for thiolate Ni^{III} species consistent with the experimental data. Interestingly, we observed that the conversion of one thiolate by a thioether apparently leads to an increased participation of the remaining thiolate in the SOMO, and consequently to a decrease of its metal character (20% of S and 67% of Ni in $\mathbf{2(CH_3CN)^{2+}}$). Indeed, in the case of the dithiolate N_2S_2 Ni^{III} complex studied by Brunold et al.[30] and of the dithiolate N_3S_2 $[Ni^{III}L(im)]^+$ previously described by us,[32] the metal character of the SOMO is more pronounced (80% and 76%, respectively) and the thiolate participation is smaller (4% and 15%, respectively).

Finally, we have also shown that complex $\mathbf{1}$ presents catalytic reductive dehalogenation activity. Such activity is of great interest since it can be used for decontaminating soil and water from chlorinated solvents. Indeed, even if a huge number of methodologies has been developed for this purpose in recent years, electrochemical reductive methods of organic halides represent a promising approach as they are intrinsically milder, more selective, and easier to implement that most of the other methods.[52] The ability of Ni complexes to mediate homogeneous reductive dehalogenation of chlorinated products has already been reported, but, up to now, mainly by a chemical agent as sodium borohydride.[53] The capability of $\mathbf{1}$ to catalytically reduce halogenated compounds, *via* an electrochemical method, is therefore promising. However, the mechanism should be investigated in detail and the efficiency of the complex evaluated. Is complex $\mathbf{1}$ active at low concentration of halogenated derivatives? Is it capable of reducing other organic halides besides CH_2Cl_2? Works are in progress in our laboratory to answer these questions.

EXPERIMENTAL SECTION

General. The ligand L[54] and the complex [NiL] (**1**)[32] were prepared according to reported methods. The synthesis of [NiL^{Me}]I (**2I**) was performed under argon (Schlenk techniques). The solvents used for electrochemical and spectroelectrochemical analyses (acetonitrile, Rathburn, HPLC grade, dichloromethane, Carlo Erba reactifs-SDS, anhydrous, and DMF, Sigma Aldrich, anhydrous, 99.8%) and the electrolyte tetrabutylammonium hexafluorophosphate (Bu_4NPF_6) were used as received and stored in a glovebox.

Synthesis of [NiL^{Me}]I (2I). Iodomethane (24 μL, 0.385 mmol) was added to a suspension of **1** (200 mg, 0.314 mmol) in dichloromethane (30 mL). The mixture was stirred overnight, giving a brown solution. The solvent was removed under vacuum, and the product was extracted from the residual solid with an excess of acetonitrile. The solvent was removed in vacuo, and THF (5 mL) was added to the residue. After a few minutes of stirring, a brown precipitate was formed. It was filtered, washed with THF (3 mL), and redissolved in a minimum volume of dichloromethane. Diethyl ether was allowed to slowly diffuse into this solution to afford a brown-orange microcrystalline solid after 24 h. This was filtered, washed with diethyl ether, and dried (**2I**, 181 mg, 0.232 mmol, 74%). IR (cm^{-1}): 3053 m, 2922w, 1956w, 1886w, 1808w, 1603s, 1569 m, 1489s, 1443s, 1265w, 1186w, 1126w, 1034w, 980 m, 748s, 698vs, 602 m. ^{1}H NMR (400 MHz, CD_3CN): δ 3.56 (s, 2H, CH_2), 3.77 (s, 2H, CH_2), 4.64 (s br, 3H, CH_3), 7.10 (t, J = 7.1 Hz, 2H, CH Ph), 7.28 (m, 6H, CH Ph), 7.39 (d, J = 7.4 Hz, 4H, CH Ph), 7.44 (t, J = 7.0 Hz, 4H, CH Ph), 7.58 (d, J = 7.2 Hz, 4H, CH Ph), 8.00 (t, J = 7.4 Hz, 1H, CH bpy), 8.07 (t, J = 7.7 Hz, 1H, CH bpy), 8.25 (br, 1H, CH bpy), 8.34 (br, 1H, CH bpy), 9.31 (br, 1H, CH bpy), 10.16 (br, 1H, CH bpy). ESI-MS (CH_3CN, m/z, I%): 651.2, 100 2^+. Anal. Calcd for $C_{39}H_{33}N_2S_2NiI \cdot H_2O$ (797.43): C, 58.74; H, 4.42; N, 3.51. Found: C, 58.73; H, 4.24; N, 3.33. Brown single crystals of **2I** · $2H_2O$ suitable for X-ray diffraction were obtained by slow evaporation of a THF/CH_2Cl_2 (1/1) solution of the product.

Synthesis of [NiL^{Me}](CF$_3$SO$_3$) (2OTf). **2OTf** was obtained quantitatively by reacting **2I** with an equimolar amount of $Ag(CF_3SO_3)$ in CH_3CN. The AgI precipitate that formed was filtered off, and the resulting solution was evaporated to dryness to give a brown powder corresponding to **2OTf** (yield: 95%). ^{1}H NMR (400 MHz, CD_3CN): δ 2.94 (s br, 3H, CH_3), 4.00 (s, 2H, CH_2), 4.11 (s, 2H, CH_2), 7.16 (t, J = 7.3 Hz, 2H, CH Ph), 7.27 (t, J = 7.6 Hz, 4H, CH Ph), 7.32 (t, J = 7.4 Hz, 2H, CH Ph), 7.42 (m, 5H, 4 CH Ph + 1 CH bpy), 7.49 (m, 5H, 4 CH Ph + 1 CH bpy), 7.57 (d, J = 7.8 Hz, 4H, CH Ph), 7.80 (t, J = 7.9 Hz, 1H, CH bpy), 7.91 (t, J = 7.9 Hz, 1H, CH bpy), 8.32 (d br, 1H, CH bpy), 8.47 (br, 1H, CH bpy).

Physical Measurements. The infrared spectra were recorded on a Magna-IR TM 550 Nicolet spectrometer as KBr pellet. ^{1}H NMR spectra were recorded on a Bruker Avance 400 MHz spectrometer. Resonance assignments were achieved from the analysis of ^{1}H−^{1}H COSY experiments. Electronic absorption spectra were recorded on a Varian Cary 100 absorption spectrophotometer in quartz cells. X-band EPR spectra were recorded on a Bruker EMX, equipped with the ER-4192 ST Bruker cavity and an ER-4131 VT at 100 K. The elemental analyses were carried out with a C, H, N analyzer (SCA, CNRS). ESI-MS experiments were performed on a Bruker Esquire 3000 Plus ion trap spectrometer equipped with an electrospray ion source (ESI). The simulations of the EPR spectra were performed by the EasySpin software.[55] The sample was analyzed in positive ionization mode by direct perfusion in the ESI-MS interface (ESI capillary voltage 2 kV, sampling cone voltage 40 V).

X-ray Crystallography. A summary of data collection and structure refinement for **2I** is reported in Table S1. Single-crystal diffraction data were taken using an Oxford-Diffraction Xcallibur S Kappa geometry diffractometer (Mo K radiation, graphite monochromator, λ 0.710 73 Å) at 150 K. An absorption correction was applied using the ABSPACK Oxford-diffraction program[56] with transmission factors in the range 0.623−0.940. The molecular structure of **2I** was solved by direct methods and refined on F^2 by full matrix least-squares techniques using the SHELXTL package.[57] All non-hydrogen atoms were refined anisotropically, and hydrogen atoms were placed at their calculated position. The structure contains four cocrystallized water molecules per two complexes, 1.5 being on symmetric elements and 2.5 disordered.

Electrochemistry. Electrochemical measurements were carried out under an argon atmosphere (in glovebox at room temperature or by argon purging at low temperature). Cyclic voltammetry and controlled potential electrolysis experiments were performed by using an EG&G model 173 potentiostat/galvanostat equipped with a PAR model universal programmer and a PAR model 179 digital coulometer. A standard three-electrode electrochemical cell was used. Potentials were referred to an Ag/0.01 M $AgNO_3$ reference electrode in CH_3CN + 0.1 M Bu_4NClO_4. Measured potentials were calibrated through the use of an internal Fc/Fc$^+$ standard. The working electrode was a vitreous carbon disk (3 mm in diameter) polished with 2 μm diamond paste (Mecaprex Presi) for cyclic voltammetry (Ep_a, anodic peak potential; Ep_c, cathodic peak potential; $E_{1/2}$ = (Ep_a + Ep_c)/2; ΔEp = Ep_a − Ep_c). Exhaustive electrolyses were carried out on reticulated vitreous carbon electrode 45 PPI (the electrosynthesis Co. Inc.) (1 cm^3). The auxiliary electrode was a Pt wire in DMF, CH_3CN, or CH_2Cl_2 + 0.1 M Bu_4NPF_6 solution.

Computational Details. Theoretical calculations were based on density functional theory (DFT) and have been performed with the ORCA program package.[58] Full geometry optimizations were carried out for all complexes using the GGA functional BP86[59−61] in combination with the TZV/P[62] basis set for all atoms and by taking advantage of the resolution of the identity (RI) approximation in the Split-RI-J variant[63] with the appropriate Coulomb fitting sets.[64] The structure optimizations of the Ni^{I} and Ni^{III} complexes were both initiated from the X-ray structure of **1** and **2I**, respectively. Increased integration grids (Grid4 in ORCA convention) and tight SCF convergence criteria were used. For all molecular property calculations, solvent effects were accounted for according to the experimental conditions. For that purpose, we used the DMF (ε = 38.3), CH_2Cl_2 (ε = 9.08), and acetonitrile (ε = 36.6) solvents within the framework of the conductor like screening (COSMO) dielectric continuum approach.[65] EPR parameters were obtained from additional single-point calculations using the hybrid functional B3LYP.[66,67] For these calculations, we employed three types of basis sets: (i) Kutzelnigg's NMR/EPR (IGLO-III) basis set[68] for all ligating N atoms, (ii) Ahlrichs' valence triple-basis set[69] with two sets of polarization functions (TZVPP)[70] for the Ni and S atoms, and (iii) Ahlrichs' valence triple-basis set[69] with one set of polarization functions (TZVP)[70] for all remaining atoms. Special care was also taken to ensure accurate results by increasing the size of the integration grid to 7 (ORCA convention) for the metal center.[71] Optical properties were also obtained from additional single-point calculations using the B3LYP[66,67] functional with the TZVP[62] basis set. Electronic transition energies and dipole moments for all models were calculated using time-dependent DFT (TD-DFT)[72−74] within the Tamm−Dancoff approximation.[75,76] To increase computational efficiency, the RI approximation[77] was used in calculating the Coulomb term and at least 30 excited states were calculated in

ASSOCIATED CONTENT

Supporting Information. Additional structural (2^+), electrochemical (**1** and 2^+), and theoretical data.This material is available free of charge via the Internet at http://pubs.acs.org.

AUTHOR INFORMATION

Corresponding Author

*E-mail: marie-noelle.collomb@ujf-grenoble.fr (M.-N.C.), carole.duboc@ujf-grenoble.fr (C.D.).

Present Addresses

[⊥]Laboratoire de Spectrochimie Infrarouge et Raman, CNRS LASIR-UMR 8516, Bat C4 F-59655 Villeneuve d'Ascq Cedex, France.

■ ACKNOWLEDGMENT

M.G. thanks the CNRS for his postdoctoral fellowship. Frank Reikowski and Eckhard Bill are acknowledged for EPR experiments. F.N. gratefully acknowledges the University of Bonn and the Max-Planck society (via a Max-Planck fellowship) for financial support of this work. Furthermore, the special research unit SFB 813 (Chemistry at Spin-Centers, University of Bonn) is gratefully acknowledged.

■ REFERENCES

(1) Ragsdale, S. W. *J. Biol. Chem.* **2009**, *284*, 18571–18575.
(2) Miller, A. F. *Curr. Opin. Chem. Biol.* **2004**, *8*, 162–168.
(3) Bryngelson, P. A.; Maroney, M. J. In *Nickel and Its Surprising Impact in Nature*; Sigel, A., Sigel, H., Sigel, R. K. O., Eds.; John Wiley & Sons Ltd.: West Sussex, U.K., 2007; pp 417−444.
(4) Barondeau, D. P.; Kassmann, C. J.; Bruns, C. K.; Tainer, J. A.; Getzoff, E. D. *Biochemistry* **2004**, *43*, 8038–8047.
(5) Wuerges, J.; Lee, J.-W.; Yim, Y.-I.; Yim, H.-S.; Kang, S.-O.; Djinovic Carugo, K. *Proc. Natl. Acad. Sci. U.S.A.* **2004**, *101*, 8569–8574.
(6) Lubitz, W.; Gastel, M. V.; Gärtner, W. In *Nickel and Its Surprising Impact in Nature*; Sigel, A., Sigel, H., Sigel, R. K. O., Eds.; John Wiley & Sons Ltd.: West Sussex, U.K., 2007; pp 279−322.
(7) Vignais, P. M.; Billoud, B. *Chem. Rev.* **2007**, *107*, 4206–4272.
(8) Garcin, E.; Vernede, X.; Hatchikian, E. C.; Volbeda, A.; Frey, M.; Fontecilla-Camps, J. C. *Structure* **1999**, *7*, 557–566.
(9) Ragsdale, S. W.; Pierce, E. *Biochim. Biophys. Acta* **2008**, *1784*, 1873–1898.
(10) Dobbek, H.; Svetlitchnyi, V.; Gremer, L.; Huber, R.; Meyer, O. *Science* **2001**, *293*, 1281–1285.
(11) Drennan, C. L.; Heo, J. Y.; Sintchak, M. D.; Schreiter, E.; Ludden, P. W. *Proc. Natl. Acad. Sci. U.S.A.* **2001**, *98*, 11973–11978.
(12) Doukov, T. I.; Blasiak, L. C.; Seravalli, J.; Ragsdale, S. W.; Drennan, C. L. *Biochemistry* **2008**, *47*, 3474–3483.
(13) Doukov, T. I.; Iverson, T. M.; Seravalli, J.; Ragsdale, S. W.; Drennan, C. L. *Science* **2002**, *298*, 567–572.
(14) Darnault, C.; Volbeda, A.; Kim, E. J.; Legrand, P.; Vernede, X.; Lindahl, P. A.; Fontecilla-Camps, J. C. *Nat. Struct. Biol.* **2003**, *10*, 271–279.
(15) Bouwman, E.; Reedijk, J. *Coord. Chem. Rev.* **2005**, *249*, 1555–1581.
(16) Evans, D. J. *Coord. Chem. Rev.* **2005**, *249*, 1582–1595.
(17) Harrop, T. C.; Mascharak, P. K. *Coord. Chem. Rev.* **2005**, *249*, 3007–3024.
(18) Grapperhaus, C. A.; Darensbourg, M. Y. *Acc. Chem. Res.* **1998**, *31*, 451–459.
(19) Mullins, C. S.; Grapperhaus, C. A.; Frye, B. C.; Wood, L. H.; Hay, A. J.; Buchanan, R. M.; Mashuta, M. S. *Inorg. Chem.* **2009**, *48*, 9974–9976.
(20) Dey, A.; Green, K. N.; Jenkins, R. M.; Jeffrey, S. P.; Darensbourg, M.; Hodgson, K. O.; Hedman, B.; Solomon, E. I. *Inorg. Chem.* **2007**, *46*, 9655–9660.
(21) Grapperhaus, C. A.; Mullins, C. S.; Kozlowski, P. M.; Mashuta, M. S. *Inorg. Chem.* **2004**, *43*, 2859–2866.
(22) Farmer, P. J.; Reibenspies, J. H.; Lindahl, P. A.; Darensbourg, M. Y. *J. Am. Chem. Soc.* **1993**, *115*, 4665–4674.
(23) Smee, J. J.; Miller, M. L.; Grapperhaus, C. A.; Reibenspies, J. H.; Darensbourg, M. Y. *Inorg. Chem.* **2001**, *40*, 3601–3605.
(24) Bellefeuille, J. A.; Grapperhaus, C. A.; Derecskei-Kovacs, A.; Reibenspies, J. H.; Darensbourg, M. Y. *Inorg. Chim. Acta* **2000**, *300*−*302*, 73–81.
(25) Grapperhaus, C. A.; Mullins, C. S.; Mashuta, M. S. *Inorg. Chim. Acta* **2005**, *358*, 623–632.
(26) Musie, G.; Reibenspies, J. H.; Darensbourg, M. Y. *Inorg. Chem.* **1998**, *37*, 302–310.
(27) Hanss, J.; Kruger, H. J. *Angew. Chem., Int. Ed.* **1998**, *37*, 360–363.
(28) Mathrubootham, V.; Thomas, J.; Staples, R.; McCraken, J.; Shearer, J.; Hegg, E. L. *Inorg. Chem.* **2010**, *49*, 5393–5406.
(29) Kruger, H. J.; Peng, G.; Holm, R. H. *Inorg. Chem.* **1991**, *30*, 734–742.
(30) Fiedler, A. T.; Brunold, T. C. *Inorg. Chem.* **2007**, *46*, 8511–8523.
(31) Fiedler, A. T.; Bryngelson, P. A.; Maroney, M. J.; Brunold, T. C. *J. Am. Chem. Soc.* **2005**, *127*, 5449–5462.
(32) Gennari, M.; Orio, M.; Pécaut, J.; Neese, F.; Collomb, M.-N.; Duboc, C. *Inorg. Chem.* **2010**, *49*, 6399–6401.
(33) Green, K. N.; Brothers, S. M.; Jenkins, R. M.; Carson, C. E.; Grapperhaus, C. A.; Darensbourg, M. Y. *Inorg. Chem.* **2007**, *46*, 7536–7544.
(34) Nakane, D.; Kuwasako, S.-i.; Tsuge, M.; Kubo, M.; Funahashi, Y.; Ozawa, T.; Ogura, T.; Masuda, H. *Chem. Commun.* **2010**, *46*, 2142–2144.
(35) Rosen, W.; Busch, D. H. *J. Am. Chem. Soc.* **1969**, *91*, 4694–4697.
(36) Ito, M.; Matsumoto, T.; Tatsumi, K. *Inorg. Chem.* **2009**, *48*, 2215–2223.
(37) Baidya, N.; Olmstead, M.; Mascharak, P. K. *Inorg. Chem.* **1991**, *30*, 929–937.
(38) Baidya, N.; Olmstead, M. M.; Mascharak, P. K. *J. Am. Chem. Soc.* **1992**, *114*, 9666–9668.
(39) Baidya, N.; Olmstead, M. M.; Whitehead, J. P.; Bagyinka, C.; Maroney, M. J.; Mascharak, P. K. *Inorg. Chem.* **1992**, *31*, 3612–3619.
(40) Gomez, L.; Pereira, E.; de Castro, B. *J. Chem. Soc., Dalton Trans.* **2000**, 1373–1379.
(41) In contrast to $\mathbf{2}^{+}$, the neutral **1** complex has been studied in DMF since it is insoluble in CH_3CN.
(42) Burke, J. A.; Brink, E. C. *Inorg. Chem.* **1969**, *8*, 386–387.
(43) Shoup, J. C.; Burke, J. A. *Inorg. Chem.* **1973**, *12*, 1851–1855.
(44) Ashby, M. T.; Enemark, J. H.; Lichtenberger, D. L. *Inorg. Chem.* **1988**, *27*, 191–197.
(45) Maroney, M. J.; Choudhury, S. B.; Bryngelson, P. A.; Mirza, S. A.; Sherrod, M. J. *Inorg. Chem.* **1996**, *35*, 1073–1076.
(46) In this manuscript, all redox potential are referred to Fc/Fc^{+}.
(47) Lovecchio, F. V.; Gore, E. S.; Busch, D. H. *J. Am. Chem. Soc.* **1974**, *96*, 3109–3118.
(48) Gagne, R. R.; Ingle, D. M. *Inorg. Chem.* **1981**, *20*, 420–425.
(49) Lappin, A. G.; McAuley, A. *Adv. Inorg. Chem.* **1988**, *32*, 241–295.
(50) Ge, P.; Riordan, C. G.; Yap, G. P. A.; Rheingold, A. L. *Inorg. Chem.* **1996**, *35*, 5408–5409.
(51) Yamamura, T.; Sakurai, S.; Arai, H.; Miyamae, H. *J. Chem. Soc., Chem. Commun.* **1993**, 1656–1658.
(52) Laine, D. F.; Cheng, I. F. *Microchem. J.* **2007**, *85*, 183–193.
(53) Alonso, F.; Beletskaya, I. P.; Yus, M. *Chem. Rev.* **2002**, *102*, 4009–4092.
(54) Kopf, M. A.; Varech, D.; Tuchagues, J. P.; Mansuy, D.; Artaud, I. *J. Chem. Soc., Dalton Trans.* **1998**, 991–998.
(55) Stoll, S.; Schweiger, A. *J. Magn. Reson.* **2006**, *178*, 42–55.
(56) *ABSPACK CrysAlis PRO RED*; Oxford Diffraction Ltd: Abingdon, Oxfordshire, U.K., 2010.
(57) Sheldrick, G. M. *SHELXTL-Plus, Structure Determination Software Programs (Version 5.1.)*; Madison, WI, 1998.
(58) Neese, F. *ORCA—An Ab Initio, Density Functional and Semiempirical Program Package (v. 2.6−35)*; Universität Bonn: Bonn, Germany, 2007.
(59) Perdew, J. P. *Phys. Rev. B* **1986**, *33*, 8822–8824.
(60) Perdew, J. P. *Phys. Rev. B* **1986**, *34*, 7406–7406.
(61) Becke, A. D. *Phys. Rev. A* **1988**, *38*, 3098–3100.

(62) Schäfer, A.; Huber, C.; Ahlrichs, R. *J. Chem. Phys.* **1994**, *100*, 5829–5835.
(63) Neese, F. *J. Comput. Chem.* **2003**, *24*, 1740–1747.
(64) Weigend, F. *Phys. Chem. Chem. Phys.* **2006**, *8*, 1057–1065.
(65) Klamt, A.; Schürmann, G. *J. Chem. Soc., Perkin Trans. 2* **1993**, 799–805.
(66) Becke, A. D. *J. Chem. Phys.* **1993**, *98*, 5648–5652.
(67) Lee, C. T.; Yang, W. T.; Parr, R. G. *Phys. Rev. B* **1988**, *37*, 785–789.
(68) Kutzelnigg, W.; Fleischer, U.; Schindler, M. In *The IGLO Method: Ab Initio Calculation and Interpretation of NMR Chemical Shifts and Magnetic Susceptibilities*; Springer-Verlag: Heidelberg, 1990; Vol. 23.
(69) Schäfer, A.; Horn, H.; Ahlrichs, R. J. *Chem. Phys.* **1992**, 2571–2577.
(70) Ahlrichs, R. Unpublished results.
(71) Neese, F. *Inorg. Chim. Acta* **2002**, *337*, 181–192.
(72) Casida, M. E. In *Recent Advances in Density Functional Methods*; Chong, D. P., Ed.; World Scientific: Singapore, 1995.
(73) Stratmann, R. E.; Scuseria, G. E.; Frisch, M. J. *J. Chem. Phys.* **1998**, *109*, 8218–8224.
(74) Bauernschmitt, R.; Ahlrichs, R. *Chem. Phys. Lett.* **1996**, 454 464.
(75) Hirata, S.; Head-Gordon, M. *Chem. Phys. Lett.* **1999**, *314*, 291–299.
(76) Hirata, S.; Head-Gordon, M. *Chem. Phys. Lett.* **1999**, *302*, 375–382.
(77) Neese, F.; Olbrich, G. *Chem. Phys. Lett.* **2002**, 170–178.